# Alkali-Metal-Mediated Reversible Chemical Hydrogen Storage Using Seawater

Pankaj Sharma,[†] Jinhyup Han,[†] Jaehyun Park,[†] Dong Yeon Kim,[†] Jinho Lee, Dongrak Oh, Namsu Kim, Dong-Hwa Seo,* Youngsik Kim,* Seok Ju Kang,* Soo Min Hwang,* and Ji-Wook Jang*

Cite This: *JACS Au* 2021, 1, 2339−2348

Read Online

ACCESS | Metrics & More | Article Recommendations | Supporting Information

**ABSTRACT:** The economic viability and systemic sustainability of a green hydrogen economy are primarily dependent on its storage. However, none of the current hydrogen storage methods meet all the targets set by the US Department of Energy (DoE) for mobile hydrogen storage. One of the most promising routes is through the chemical reaction of alkali metals with water; however, this method has not received much attention owing to its irreversible nature. Herein, we present a reconditioned seawater battery-assisted hydrogen storage system that can provide a solution to the irreversible nature of alkali-metal-based hydrogen storage. We show that this system can also be applied to relatively lighter alkali metals such as lithium as well as sodium, which increases the possibility of fulfilling the DoE target. Furthermore, we found that small (1.75 cm$^2$) and scaled-up (70 cm$^2$) systems showed high Faradaic efficiencies of over 94%, even in the presence of oxygen, which enhances their viability.

**KEYWORDS:** alkali metals, electrocyclic reactions, hydrogen storage, reversible process, seawater battery

## ■ INTRODUCTION

Hydrogen is the most abundant element in the universe, possessing more than three times the chemical energy (142 MJ kg$^{-1}$) of other liquid hydrocarbon fuels (47 MJ kg$^{-1}$) which makes it a promising future energy carrier.[1,2] However, hydrogen storage is a significant problem because current commercial hydrogen storage systems, such as compression (350−700 bar at room temperature) and liquefaction (−253 °C, 5−10 bar) systems, consume high energy and also present safety issues.[1] Therefore, to enable the evolution of hydrogen-fueled vehicles, stationary power, and portable electronic devices, innovative technologies capable of storing significant amounts of hydrogen are necessary, while considering their high volumetric and gravimetric density under ambient temperature and pressure conditions.[3] Apart from high-efficiency hydrogen storage, the system should also exhibit reversibility (hydrogenation and dehydrogenation) and a long lifespan.[4,5] The US Department of Energy (DoE) has set a target of fabricating a system that can achieve 6.5 wt % and 50 g L$^{-1}$ hydrogen storage capacities for the operating conditions of 12 bar (adsorption)/3 bar (desorption), 85 °C (adsorption)/~40 °C (desorption), and almost 1500 operational cycles.[6]

To achieve this goal, in the last couple of decades, researchers worldwide have explored new technologies for hydrogen storage and potential materials, such as metal hydrides,[7−10] chemical hydrides,[11−15] porous carbon materials,[16−19] metal−organic frameworks,[20−23] covalent organic frameworks,[24−26] and alkali metals,[27] as well as traditional storage techniques such as compression[28] and liquefaction[29] of hydrogen gas. Despite these exceptional and innovative findings, we are still far from making the hydrogen economy a sustainable and economically viable energy carrier, and none of these hydrogen storage methods are considered ideal for hydrogen energy carriers.

The chemical reaction of alkali metals with water is a promising hydrogen storage route, but this storage process has received minimal research attention because of its irreversible nature.[4,27,30] The most advantageous feature of a hydrogen storage system that uses an alkali-metal-based chemical reaction (eq 1) is that the hydrogen fuel can be stored at ambient temperature (25 °C) and atmospheric pressure (1 atm), along with a high gravimetric capacity (4−14 wt %) and exceptional volumetric capacity (42−218 g L$^{-1}$), which can easily surpass the respective ultimate targets of 6.5 wt % and 50 g L$^{-1}$ set by the DoE.
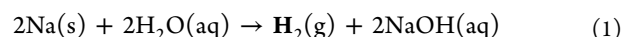
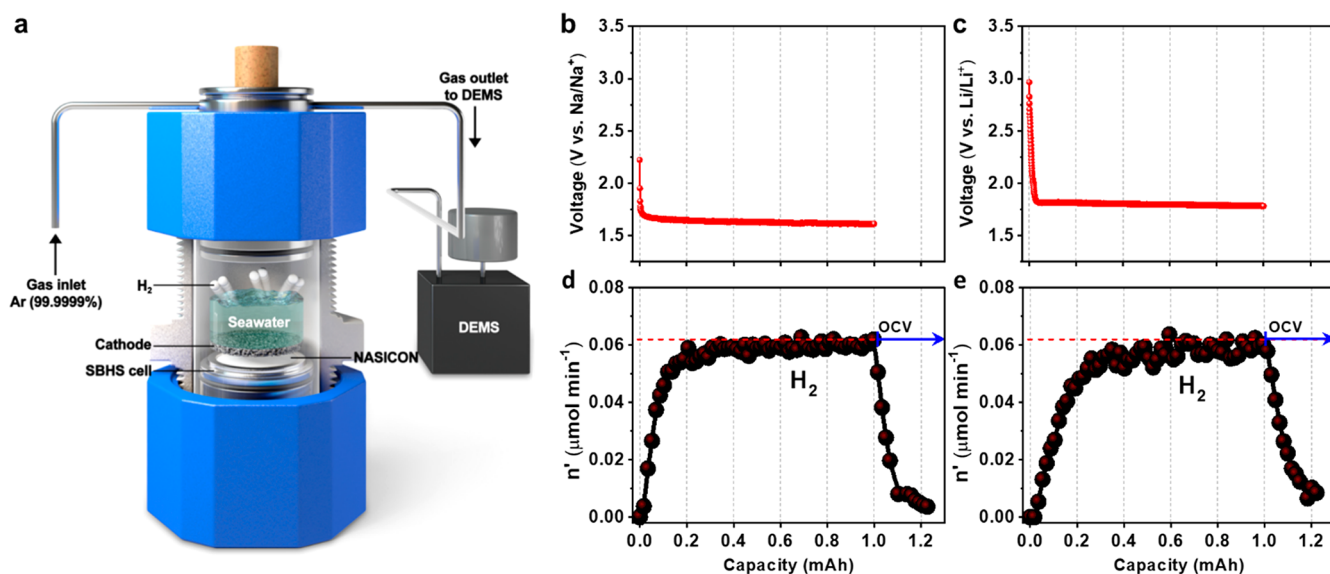$$2Na(s) + 2H_2O(aq) \rightarrow \mathbf{H_2}(g) + 2NaOH(aq) \tag{1}$$
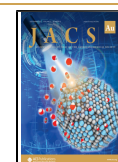
**Figure 1.** Hydrogen storage performance of Na- and Li metal-based SBHS coin cells. (a) Schematic representation of the Swagelok-type seawater battery system. (b,c) 0.1 mA cm$^{-2}$ galvanostatic discharge voltage profile of (b) Na metal (anode)/seawater (cathode) and (c) Li metal (anode)/ 0.5 M Li$_2$SO$_4$ aqueous electrolyte. (d,e) In situ differential electrochemical mass spectrometry (DEMS) results of the cell containing (d) Na metal/ seawater and (e) Li metal/0.5 M Li$_2$SO$_4$ aqueous electrolyte. Both cells showed vigorous hydrogen gas evolution during discharge.

This chemical approach provides a new perspective and a simpler way to store and transport hydrogen, which can ultimately make a hydrogen economy more viable. The single major drawback of the alkali-metal-based (chemical) hydrogen storage process is its irreversibility, which signifies the inability of the system to regenerate the alkali metals for reuse. Although Na can be recovered by the electrolysis of a molten sodium salt, this process is not commercially viable or energy efficient (requiring approximately 330 °C and 9700 kWh power for producing 1 ton of Na).[30,31] Furthermore, alkali metal storage is a significant issue, as alkali metals readily form metal oxides and hydroxides when they are exposed to air and moisture, respectively. Therefore, they require special protection during regeneration, storage, and usage.

Herein, we present a reconditioned seawater battery system as a highly reversible chemical hydrogen storage system (Figure S1), where alkali metals are harvested during charging (eq 2) and hydrogen gas is collected during the discharging process under ambient conditions (eq 1) (Note S1, Figures S1 and S2b).
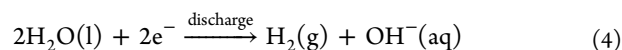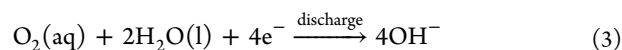
$$2NaOH(aq) \rightarrow 2\textbf{Na}(s) + \frac{1}{2}O_2(aq) + H_2O(l) \qquad (2)$$
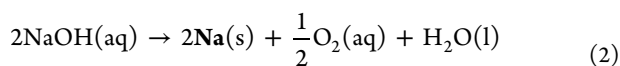
The faradaic efficiency (FE) of 99.7% obtained during the discharging process (discharging current density 0.1 mA cm$^{-2}$) of hydrogen collection under Ar atmosphere demonstrates a feasible transformation of abundant seawater into a reversible and sustainable hydrogen storage system. In this study, we also substantiate the compatibility of the reported seawater battery-based hydrogen storage system with another alkali-metal-based anodic cell (such as Li) to further increase the hydrogen storage capacity. Furthermore, the charging and discharging voltages can be easily tuned by changing the anode from Na to FeS$_2$. Notably, even in the presence of O$_2$, the seawater battery hydrogen storage (SBHS) system explicitly yields FE values of 99.1% and 94.7% for the seawater battery coin cell (1.75 cm$^2$) and the scaled up prismatic double-side seawater battery (70 cm$^2$), respectively, at high discharge currents. The high FE

values of the SBHS system under ambient conditions were elucidated using density functional theory (DFT) with suitable computational models.

## RESULTS AND DISCUSSION

Seawater batteries use natural seawater to store and supply energy through redox reactions.[32−34] Unlike traditional rechargeable batteries (such as lithium ion, sodium ion, nickel−metal hydride, lead acid, etc.), seawater batteries are based on an open-structured cathode compartment, which allows gaseous O$_2$ from the ambient air to enter seawater (aerated) (Figure S3a,b). Thus, the O$_2$ reduction reaction (eq 3) predominantly occurs under these conditions (Figure S3bI). Conversely, the SBHS system discharges in O$_2$-deficient (deaerated) conditions, producing electric power and hydrogen gas using the seawater through a water reduction reaction (eq 4).

$$O_2(aq) + 2H_2O(l) + 4e^- \xrightarrow{\text{discharge}} 4OH^- \qquad (3)$$

$$2H_2O(l) + 2e^- \xrightarrow{\text{discharge}} H_2(g) + OH^-(aq) \qquad (4)$$

To verify and quantify hydrogen gas production during discharge under O$_2$-deficient conditions, in situ differential electrochemical mass spectrometry (DEMS) analysis was conducted.[35] Subsequently, we collected the evolved gas from a homemade Swagelok-type cell shown in Figure 1a. Using a modified coin-type cell with a controlled Ar environment during the discharge process enabled us to monitor hydrogen gas evolution during the discharging process. Figure 1b illustrates the first galvanostatic discharge trajectory of the Na/NASICON/Seawater architecture cell at a constant current density of 0.1 mA cm$^{-2}$.

The stable plateau at 1.62 V implied a unique electro-chemical reaction under Ar gas, in which the potential did not match the conventional discharge voltage of a seawater battery in an air environment. This potential can be explained by the evolution of hydrogen gas from seawater. When the cell was
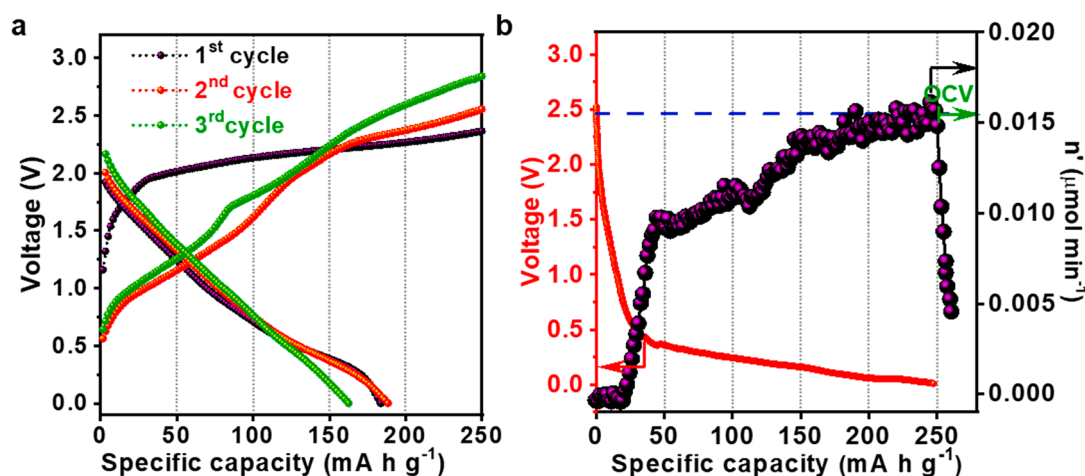
**Figure 2.** SBHS with reduced operation voltage and its hydrogen storage performance. (a) Charge−discharge voltage profiles of the seawater coin-cell at a current rate of 0.01 mA cm$^{-2}$(FeS$_2$/seawater). (b) Discharge voltage trajectory (black) and in situ DEMS result for galvanostatic discharge at a fixed current density of 0.025 mA cm$^{-2}$.

filled with inert Ar gas, it resulted in hydrogen gas evolution during discharge. The evolution of hydrogen gas was further quantified by the DEMS measurements. Specifically, the obtained value of 0.06 $\mu$mol min$^{-1}$ (Figure 1d) indicates that the electrochemical reaction (eq 4) had an observed hydrogen gas evolution rate close to the theoretical value of 0.062 $\mu$mol min$^{-1}$ (95% of FE). Hydrogen collection during the discharge process was further confirmed at a low discharge current density of 0.05 mA cm$^{-2}$ using natural seawater (Figure S4) and 0.5 M Na$_2$SO$_4$ aqueous electrolyte (Figure S5), yielding FE values of 99.7% and 91.8%, respectively. Moreover, this hydrogen storage system was versatile, with many possibilities for advancement, one of which was by changing anode materials and using other metal systems (Figure 1 and Figure S6). A similar system, where the Na anode is was replaced by a lithium anode, also exhibited remarkable performance in terms of hydrogen generation and showed an FE of 90.2% (Figure 1e and Figure S6b) at a discharge voltage of 1.79 V (Figure 1c). In particular, lithium has high gravimetric (14 wt %) and volumetric capacities (77.6 g L$^{-1}$), both of which are far higher than the DoE targets for onboard hydrogen storage.[6]

Notably, the potential window of the general SBHS system is 1.6−3.8 V vs Na$^+$/Na, and it can be easily regulated by simply replacing the Na anode with a different anode. This indicates that the ratio of the electrical energy requirement and hydrogen energy collection during charging is highly controllable, and the charging voltage can be reduced further, making self-charging using solar energy more feasible. Here, we decreased the operating voltage of the system from 1.6−3.8 V vs Na$^+$/Na to a potential window of 0.5−2.5 V vs Na$^+$/Na for sodiation/desodiation by replacing the Na anode with a FeS$_2$ electrode.[36,37] The X-ray diffraction (XRD) pattern and scanning electron microscopy (SEM) image of the microscale FeS$_2$ powder are shown in Figure S7. The galvanostatic charge and discharge voltage profiles of a half-cell with the FeS$_2$ electrode (Na|FeS$_2$) at a current rate of 0.01 mA cm$^{-2}$ and 20 mA g$^{-1}$ are reported inFigure 2a and Figure S8a, respectively. As the first irreversible cycle is due to the formation of solid-electrolyte interphase on the surface (Coulombic efficiency ∼75%), the FeS$_2$ electrode showed a good charge−discharge behavior with a specific capacity of ∼380 mAh g$^{-1}$ during

subsequent cycles (Figure S8b). We then employed the FeS$_2$ electrode as the anode in the SBHS system and cycled the system at a current density of 0.01 and 0.05 mA cm$^{-2}$ (Figure S9a), with a capacity cutoff (250 mAh g$^{-1}$, anode) on charging and a voltage cutoff (0 V) on discharging (Figure 2b). The corresponding DEMS measurement result indicated the evolution of a large amount of hydrogen gas, with FE values of 83.9% (Figure S8c) and 74.9% (Figure S9c). Although the FE was lower than that of the Na anode (Figure 1d), the results clearly indicated that the FeS$_2$ anode is feasible for the SBHS system. The operation voltage for the FeS$_2$-based SBHS system decreased over 1 V compared to that of the Na anode-based SBHS system (Figure S10).

Subsequently, we examined the operation of the SBHS system using a coin-type seawater battery cell in an a larger airtight setup (details of the laboratory-scale SBHS system construction and operation are provided in the Supporting Information and Figure S11). To analyze the electrochemical and hydrogen storage performance of the SBHS system, cycling tests were performed in an O$_2$-free environment. Figure 3a presents the galvanostatic charge−discharge voltage profile of the SBHS cell at a current density of 0.25 mA cm$^{-2}$ for 6 h each. For each cycle (Figure 3a), mainly oxygen evolution and/or minor chlorine oxidation reactions occurred during charging and seawater reduction (hydrogen evolution) during discharging (Figure S2). The stable and continuous operation of the cell over 33 cycles of 400 h duration (Figure 3a,b) is indicated by the metal−water chemical reaction plateaus that appeared as a result of seawater oxidation, signifying feasible reversible hydrogen storage using this SBHS system. The average and highest FE values of hydrogen gas collected from 33 cycles in an O$_2$-free environment were estimated to be 95 and 100% (Figure 3b), respectively. To further investigate the stability of the SBHS system with more comprehensive product analysis, DEMS measurements were also conducted during the 400 h cycling test under a continuous Ar gas bubbling atmosphere at a fixed current density of 0.25 mA cm$^{-2}$ (Figures S12 and S13). The FE evaluation after 200 and 400 h of the cyclic study showed over 92% H$_2$ collection efficiency and almost overlapping charge/discharge profiles, demonstrating excellent performance and electrochemical cyclic stability. Furthermore, the pH measurements made
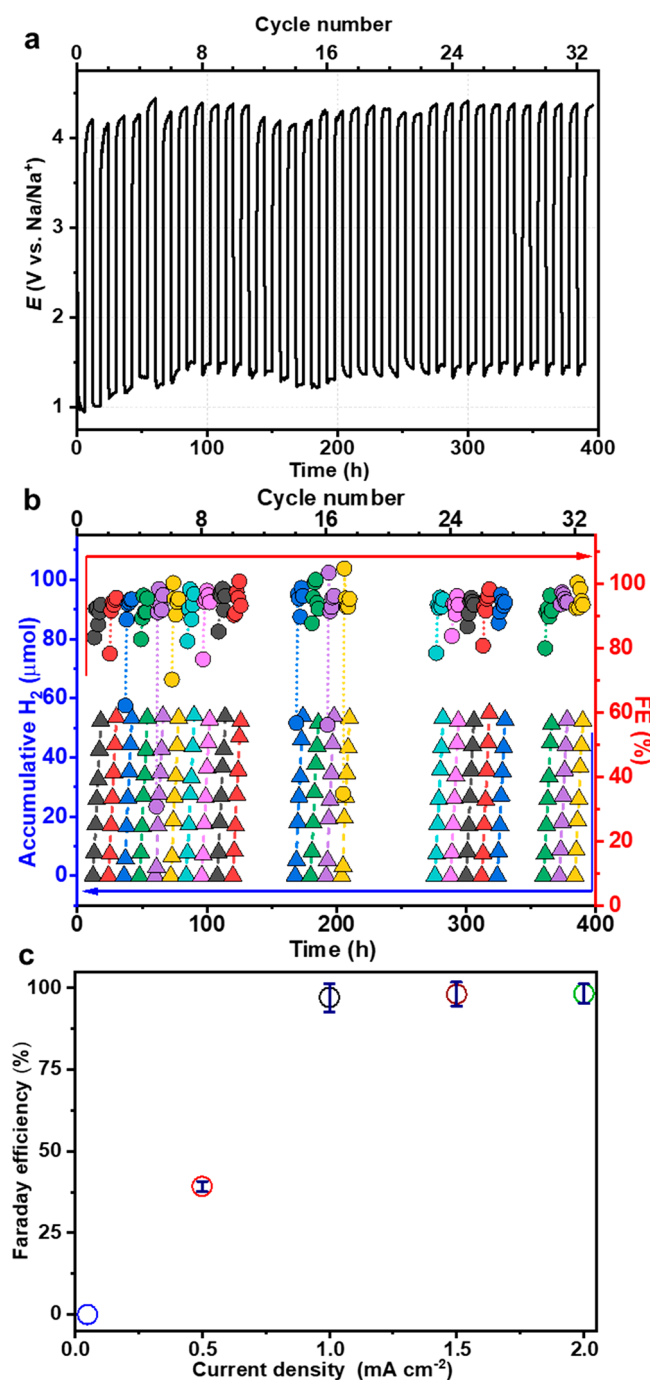
**Figure 3.** Electrochemical and hydrogen storage performance of the SBHS system. (a) Charge−discharge (6 h each) voltage profiles of the seawater coin cell at a current density of 0.25 mA cm$^{-2}$ (Na/seawater) for almost 400 h. (b) Hydrogen gas generation and the corresponding FE (%) during discharge for different cycles in O$_2$-free conditions. An online-GC system with continuous Ar gas purging at a flow rate of 10 sccm. (c) Variation in the FE as a function of the discharge current density (0.05−2.0 mA cm$^{-2}$) for collected hydrogen gas from the SBHS system during the discharging process in the presence of air. The FE values were calculated using the average of the last six consecutive points of H$_2$ quantified using online GC.

during the galvanostatic cycling studies (Figure S13b) and Cl$_2$ gas evolution monitoring (Figure S14) during the charging process highlight the insignificant change in the characteristics of seawater. Moreover, in this study, a detailed stability analysis

(NASICON and seawater battery) and an analysis on the possible interference of ionic species during SBHS operation were also performed (Figures S15−S19).

However, seawater always contains dissolved oxygen; therefore, the SBHS system must remain operational regardless of the O$_2$ content in the system in order to simulate the real hydrogen storage system in seawater. Considering this, we performed the same hydrogen gas collection experiment under ambient conditions in aerated seawater without Ar purging at different discharge current densities using a Swagelok cell (Figure 1a) and a laboratory-scale SBHS system (Figure S11). The FE and time profile hydrogen gas collection results for both of these reaction cells are shown reported in Figure 3b and Figures S20 and S21. The cumulative hydrogen gas collection concentration and FE (%) results obtained from the Swagelok-type cell reported in Figure S20 demonstrate the potential utility of the SBHS system for practical utilization. The initially observed FE during discharging at 0.05 mA cm$^{-2}$ was only ∼15.3% (Figure S20). However, an increase in the discharge current density from 0.2 to 0.5, 1.0, 1.5, and 2.0 mA cm$^{-2}$ resulted in a dramatic increase in the FE values from ∼38% to 71%, 93%, 94%, and 99% (Figure S20), respectively. These results demonstrate that the FE for hydrogen gas collection was enhanced by maintaining a high discharge current in aerated seawater (Figure S20). At a low discharge current, the O$_2$ in seawater is reduced, but at a high discharge current, the O$_2$ reduction in seawater starts decreasing. According to the Nernst equation (Note S1), the cell voltage (E) depends on the concentration of reactants as well as the product. Assuming natural seawater to have a pH of ∼8, Na$^+$ cation concentration of ∼0.47 M, and the activity coefficients to be unity (H$_2$O, Na$^+$, and OH$^-$), the theoretically calculated cell voltages for sodium−oxygen and sodium hydrolysis are 3.48 and 2.24 V, respectively. The concentration polarization across the electrodes due to the restricted exchange of ions/constituents decreases the cell voltage. Therefore, at a high current density, the open carbon cathode can exhaust O$_2$ to a certain limit where the cell voltage shifts to a lower value (approximately 2.24 V), which is favorable for the hydrogen evolution reaction during the discharging process (eq 4). Furthermore, during the discharging/O$_2$ reduction reaction (eq 3), the cell voltage approaches the lowest possible limit, as the polarization influence on the cell voltage is significantly higher to the reactant oxygen, whereas a slight decrease occurs during hydrogen gas generation (eq 4, a reaction product). These results also established that hydrogen gas collection in the SBHS system during discharging is also favorable for generating high current densities and sustainable technology development.[38] In parallel to the online Swagelok cell-DEMS system, hydrogen gas collection from aerated seawater was further confirmed by a relatively larger laboratory-scale SBHS system coupled with online GC quantification (Figure 3c and Figures S21 and S22). This system also exhibited good reversibility under aerated conditions at a discharge current of 1 mA cm$^{-2}$, with an FE close to 100% (Figure S22).

For practical applications of the SBHS system, maximizing the maximum use of abundant sodium metal ions that are present in the infinite medium of seawater is important for improving its scalability. We constructed a prismatic single-cell system with a 70 cm$^2$ active area, as shown in Figure 4a, using a schematic illustration as well as digital photographs. The detailed fabrication process for the sodium anode (cutting/punching of the laminate film, NASICON membrane loading,
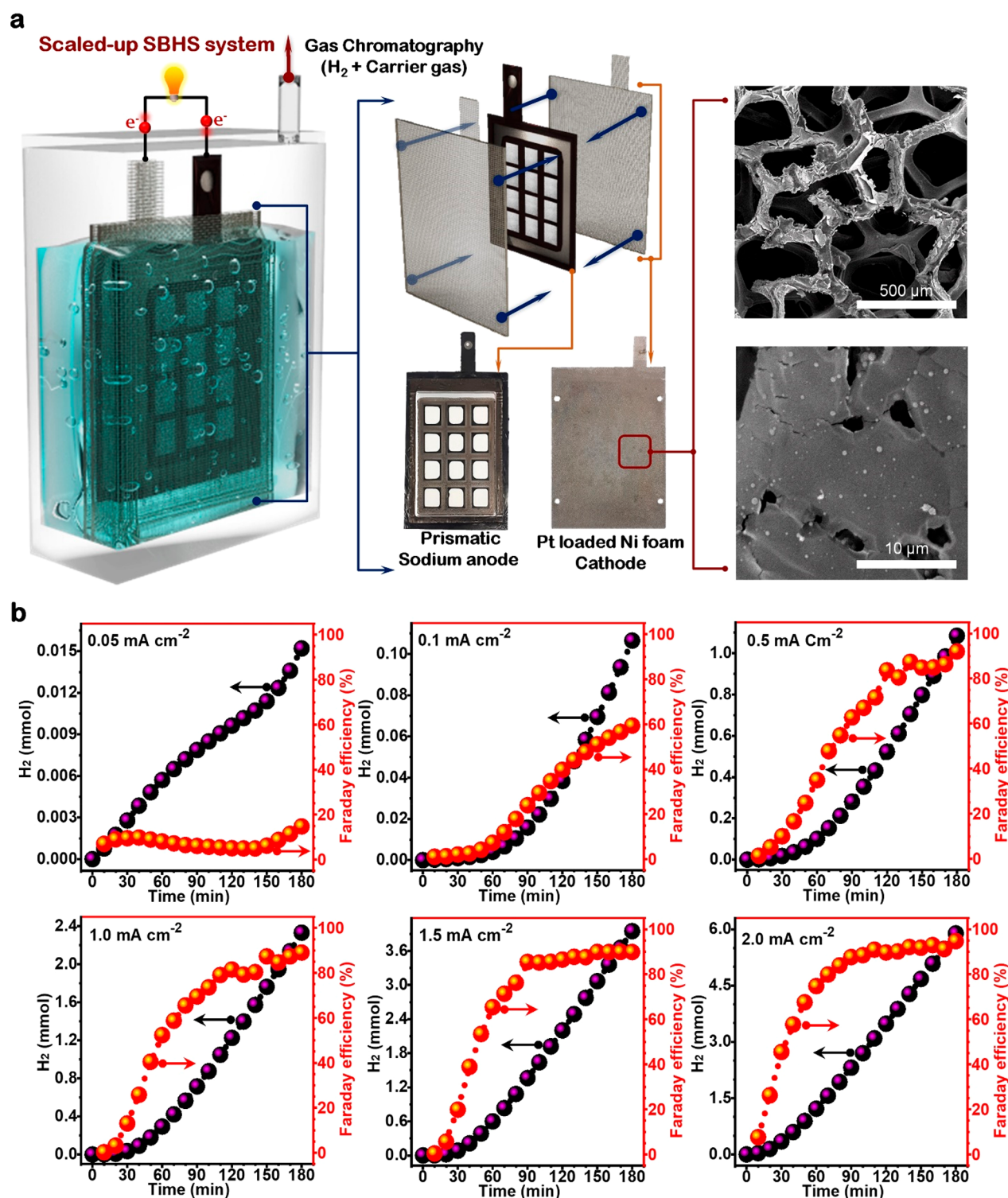
**Figure 4.** Cell stack and SBHS module construction for large-scale hydrogen storage. (a) Schematic representation of the scaled-up seawater battery system and the generic view of stepwise construction of scaled-up SBHS cell (16.5 cm × 12.0 cm) with 70 cm$^2$ active anode area for the sustainability and feasibility of hydrogen storage technique. The photographic images and SEM micrographs describe the electrodes and surface structure of Pt-loaded Ni foil cathodic part, respectively. (b) Time course hydrogen gas collection and FE data obtained from scaled-up SBHS system during the discharging process at different discharge current density values 0.05−2.0 mA cm$^{-2}$ (Na/seawater) in aerated seawater under ambient conditions.

attaching of the aluminum frame to the laminate film, electrical lead loading, inserting an anode and a nonaqueous electrolyte, sealing the cell edges, and assembling the anode compartment with a cathode current collector) has been reported elsewhere.[33,39] To evaluate its technological acceptance, operational viability, and hydrogen gas collection efficiency, separate sets of experiments were performed in aerated water under ambient conditions. Furthermore, to maximize the performance of the scaled-up SBHS system, Pt-loaded Ni foam (Pt@NiF) (16.5 cm × 12.0 cm) was used as the cathode (see Note

**Figure 5.** Theoretical calculations of two distinct cathodic reactions in the SBHS system. (a) DFT-calculated potential ($U_{SHE}$)−pH diagram for the porous carbon model, showing the reaction phase of each cathodic reaction. The red and blue dashed lines denote the ideal equilibrium states of the ORR and HER, respectively, while their corresponding solid lines denote the DFT-calculated equilibrium states of the ORR and HER, respectively. (b,c) Illustrations of reaction pathways and optimized geometries of the two-layered graphite with hole defect (Cat*; where * stands for active site) and their reaction intermediates (OOH*, O*, OH*, and H*) for the (b) ORR and (c) HER. The upper and lower layers are described by ball-and-stick and stick models, respectively, to clearly distinguish between the two layers (black/gray: C, white: H, red: O, sky-blue: H in adsorbates). (d) Schematic representations for different cathodic reactions for changing current.

S1). The SEM images (Figure 4a, inset), XRD pattern (Figure S23), and X-ray photoelectron spectroscopy (Figure S24 and S25) of the Pt@NiF cathode confirmed the loading of Pt on the nickel foam. To improve the quantification of evolved hydrogen gas, the continuous flow method was used where the evolved hydrogen gas was directly quantified using online connected gas chromatography (Figure 4a). In this scaled-up system, FE values at 0.05, 0.1, 0.5, 1.0, 1.5, and 2.0 mA cm$^{-2}$ were 14.8, 59.4, 89.2, 90.0, 90.0, and 94.7%, respectively, which shows a trend similar to that observed for DEMS and coin cells. Furthermore, the scaled-up prismatic single-cell system showed an FE of almost 90% after 1 h of discharging at 2.0 mA cm$^{-2}$, whereas the same system operating at a low discharging current density (0.05, and 0.1 mA cm$^{-2}$) did not reach the equilibration point even after 3 h of discharge (Figure 4b). This quick improvement in the FE at higher discharge current densities is most likely due to the self-degassing of the SBHS

by a faster hydrogen evolution rate during discharging. Therefore, by optimizing the reaction conditions and increasing the discharge current, we can further maximize the performance. We believe that this system can be further scaled up for the commercialization of this system for hydrogen storage.

To further understand the electrochemical reactions in the SBHS, DFT calculations were performed to address selective issues in the cathode for a changing current density (Figure 5). The computational hydrogen electrode (CHE) model devised by Nørskov and co-workers[40] was used in this study. As shown in Figure 5a, the potential−pH diagram, which represents the thermodynamically favored reaction phase as a function of standard hydrogen electrode potential ($U_{SHE}$) and pH, was constructed based on the CHE model. We used a porous carbon model[41,42] to reproduce the experimental carbon cathode, and this model was used to investigate the activities

of the oxygen reduction reaction (ORR) (Figure 5b) and hydrogen evolution reaction (HER) (Figure 5c). As shown in Figure 5a, the discharging voltage ($Na^+/Na^0$) of ORR and HER were 3.04 and 2.06 V, respectively, at pH = 8, which are in good agreement with experimental discharge voltage profiles. The optimized structures for their reaction intermediates are shown in Figure 5b,c and Figure S26 (see the computational details in Note S2). The free energy diagrams for the ORR and HER are shown in Figure S27a,b. Figure 5a shows that ORR occurs at a higher potential than HER, and the HER is restricted in the high potential region. However, the working potential gradually decreased from a high voltage to low voltage during the discharging process; therefore, we infer that ORR occurs early during the discharge process (high potential region) and that the HER is thermodynamically forbidden in that region. In addition, at a low current density, the oxygen reduction is not sufficient to surpass the oxygen feeding rate or to fully deplete the dissolved oxygen. Thus, the residual oxygen in seawater helps maintain the ORR and high voltage sufficiently long at a low current density.

In contrast, at a high current density, the system possesses sufficient power to use up all residual oxygen around the electrode surface and also shift the voltage to a lower value for HER.[43] Furthermore, we investigated the electrochemical stability of the cathode using DFT.[44] Figure S27c shows the reaction free energy with respect to the standard hydrogen electrode potential ($U_{SHE}$) at pH = 8, indicating that H* was most stable in the low-potential region. Similarly, the calculated Porubaix diagram shows the thermodynamically stable surface as a function of $U_{SHE}$ and pH (Figure S27d). As shown in the surface phase diagrams, the electrode surface was protonated (H*) in the low-potential region. The protonated surface boosts hydrogen evolution via Tafel and Heyrovsky reaction pathways[45] rather than through an oxygen-involving reaction. Hence, at high current densities, HER is thermodynamically favored, and the protonated electrode surfaces also accelerate the fast kinetics of HER, while suppressing the competing ORR kinetics.

Furthermore, a series of DFT calculations were performed using the Pt (111) surface to validate our interpretations. The Pt (111) surface can explain the electrochemical reactions of Pt@NiF because the (111) surface of Pt was prominently observed in the XRD data for Pt@NiF (Figure S24), and the nickel foam substrate was not included in the calculation model.[46,47] As shown in Figures S28 and S29, the electrochemical activities of Pt (111) were almost consistent with those of the porous carbon model. This implies that our findings for the electrochemical reactions in seawater batteries may be applicable to any cathode model.

The peculiarity of the SBHS system is that sodium is supplied from an abundant source of seawater (Figure S1). Furthermore, the reversible nature of the SBHS system makes it distinct from many other hydrogen storage materials and methods. Thus, this hydrogen storage system may be be substantially cheaper than existing systems and has immense hydrogen storage capacity. Reference seawater generally has ~3.5% salt, of which $Na^+$ constitutes 30.66%. This signifies that just 10 mile[3] of seawater has the potential to generate approximately 21.7 million tons of hydrogen by chemical means, which is twice that of the projected annual worldwide hydrogen gas consumption by 2040 (10 million tons).[48−50] As 71% of the Earth's surface is covered by oceans (almost 197 million miles[2]), rechargeable seawater batteries can be

potentially limitless hydrogen storage systems. Furthermore, the SBHS system resolves the safety issue associated with hydrogen storage, which has always been a crucial problem for the hydrogen economy, because seawater also acts as a coolant and can control the temperature and minimize the thermal risks. This decreases the cost and technical impediments, making the system substantially safer, more robust, and more efficient. Thus, the seawater-battery-assisted hydrogen storage system can serve as a new avenue for the hydrogen economy (Figure S1). Similar to the natural gas supply, the hydrogen generated in the primary system can also be distributed through pipelines to desired locations (such as factories, households, and hydrogen gas fuel stations), as shown in Figure S1. Furthermore, off-board/stationary storage (distribution hubs and refilling stations for fuel cell electric vehicles) and onboard storage (on the vehicles themselves) are also feasible; however, conventional electrolysis systems for hydrogen gas production cannot be installed in the vehicles because they are generally too large and heavy (Figure S1). To further enhance the hydrogen storage capacity and operation of the SBHS system under adverse conditions, future work will focus on designing an advanced reactor (multicompartment system), where charging and discharging will take place in a separate compartment, as schematically illustrated in Figure S1 (double cathodic compartment seawater battery design part located in seawater). The simultaneous charging and discharging of the SBHS system will help to further improve the performance. Thus, the interference of $O_2$ that is produced during charging inthe hydrogen gas evolution reaction during discharging can be eliminated. Figure S1 also highlights that the electricity generated during discharging can be used along with hydrogen storage, and it can be used for recharging the system to recover Na, which will enable an uninterrupted hydrogen gas supply.

## ■ CONCLUSIONS

In summary, we demonstrated a new concept of a reversible hydrogen storage system that operates under ambient pressure and temperature, without using costly chemicals or expensive noble metal catalysts, by simply using the abundant $Na^+$ ions in the seawater via a modified seawater battery system. The results obtained for a different anodic system (Li anode) for reversible hydrogen storage confirmed the potential of using different active mediators for hydrogen storage. Furthermore, the charging and discharging voltages were easily tuned by changing the anode from Na to $FeS_2$. Notably, even in the presence of $O_2$, the SBHS system distinctively showed FE values of 99.1% and 94.7% for seawater battery coin cell (1.75 $cm^2$) and scaled up prismatic double-side seawater battery (70 $cm^2$), respectively, at a high discharging current (2 mA $cm^{-2}$), which enhances their viability. First-principle calculations substantiated that at high current density, residual oxygen around the electrode surface was exhausted and the discharging voltage shifted to a lower value, which is favorable for HER. In addition, electrochemical stability analysis showed that protonated electrode surfaces in the low-potential region accelerated the fast kinetics of HER while suppressing the competing ORR. This system can be considered to be the safest hydrogen storage system because it does not involve a high operational temperature, extreme pressure, volatile compounds, hazardous materials, nor a thermal control system. As an alkali-metal hydrogen storage has the potential to achieve the DoE targets for an onboard system (Table S1), including those for gravimetric capacity, volumetric capacity,

temperature, pressure, and reversibility, this SBHS system can be installed in vehicles (cars, trucks, trains, etc.), as well as hydrogen gas stations. The proposed SBHS system provides a new perspective on hydrogen storage and can be considered as the most natural, safe, and simple way to achieve a hydrogen economy.

## ■ ASSOCIATED CONTENT

### Ⓢ Supporting Information

The Supporting Information is available free of charge at https://pubs.acs.org/doi/10.1021/jacsau.1c00444.

> Detailed experimental procedures, preparation of the cell components, assembly of SBHS system, operational principle, theoretical cell voltage of seawater batteries, material characterization, computational details, DFT results, Figures S1–S30, Tables S1–S3, and analytical data (PDF)

## ■ AUTHOR INFORMATION

### Corresponding Authors

**Ji-Wook Jang** − School of Energy and Chemical Engineering, Ulsan National Institute of Science and Technology (UNIST), Ulsan 44919, Republic of Korea; Emergent Hydrogen Technology R&D Center, Ulsan National Institute of Science and Technology (UNIST), Ulsan 44919, Republic of Korea; ⓞ orcid.org/0000-0003-1251-1011; Email: jiwjang@unist.ac.kr

**Soo Min Hwang** − School of Energy and Chemical Engineering, Ulsan National Institute of Science and Technology (UNIST), Ulsan 44919, Republic of Korea; SKKU Advanced Institute of Nanotechnology (SAINT), Sungkyunkwan University, Suwon 16419, Republic of Korea; ⓞ orcid.org/0000-0001-7678-5906; Email: smhwang@skku.edu

**Seok Ju Kang** − School of Energy and Chemical Engineering, Ulsan National Institute of Science and Technology (UNIST), Ulsan 44919, Republic of Korea; ⓞ orcid.org/0000-0002-9921-6674; Email: sjkang@unist.ac.kr

**Youngsik Kim** − School of Energy and Chemical Engineering, Ulsan National Institute of Science and Technology (UNIST), Ulsan 44919, Republic of Korea; ⓞ orcid.org/0000-0001-7076-9489; Email: ykim@unist.ac.kr

**Dong-Hwa Seo** − School of Energy and Chemical Engineering, Ulsan National Institute of Science and Technology (UNIST), Ulsan 44919, Republic of Korea; Email: dseo@unist.ac.kr

### Authors

**Pankaj Sharma** − School of Energy and Chemical Engineering, Ulsan National Institute of Science and Technology (UNIST), Ulsan 44919, Republic of Korea; Present Address: Cardiff Catalysis Institute, School of Chemistry, Cardiff University, Cardiff CF10 3AT, U.K. UK Catalysis Hub, Research Complex at Harwell, Rutherford Appleton Laboratory, Harwell OX11 0FA, U.K

**Jinhyup Han** − School of Energy and Chemical Engineering, Ulsan National Institute of Science and Technology (UNIST), Ulsan 44919, Republic of Korea

**Jaehyun Park** − School of Energy and Chemical Engineering, Ulsan National Institute of Science and Technology (UNIST), Ulsan 44919, Republic of Korea

**Dong Yeon Kim** − School of Energy and Chemical Engineering, Ulsan National Institute of Science and Technology (UNIST), Ulsan 44919, Republic of Korea; ⓞ orcid.org/0000-0001-7798-1108

**Jinho Lee** − School of Energy and Chemical Engineering, Ulsan National Institute of Science and Technology (UNIST), Ulsan 44919, Republic of Korea

**Dongrak Oh** − School of Energy and Chemical Engineering, Ulsan National Institute of Science and Technology (UNIST), Ulsan 44919, Republic of Korea

**Namsu Kim** − School of Energy and Chemical Engineering, Ulsan National Institute of Science and Technology (UNIST), Ulsan 44919, Republic of Korea

Complete contact information is available at:
https://pubs.acs.org/10.1021/jacsau.1c00444

### Author Contributions

P.S. and D.O. performed the hydrogen storage capacity evaluation experiments using a laboratory-scale, scaled-up SBHS system and data analysis. J.H. and J.L. fabricated the seawater battery coin cells and performed the electrochemical studies. D.Y.K. and D.-H.S. conducted DFT simulations for the electrochemical reactions of seawater batteries. S.J.K. and J.P. constructed the Swagelok-type seawater battery system to study the hydrogen storage performance and electrochemical behavior of seawater batteries. D.O. helped in the construction and performance evaluation of the scaled-up SBHS. N.K. provided the initial assistance. Y.K. provided valuable input. S.J.K., S.M.H., and J.-W. J. proposed, designed, and directed the research. P.S. wrote the manuscript. D.-H.S.,Y.K., S.J.K, S.M.H., and J.-W.J. reviewed and refined the manuscript.

### Author Contributions

†P.S., J.H., J.P., and D.Y.K. contributed equally to this work.

### Notes

The authors declare no competing financial interest.

## ■ ABBREVIATIONS

SBHS, seawater battery hydrogen storage; DoE, Department of Energy; DEMS, differential electrochemical mass spectrometry; DFT, density functional theory; CHE, computational hydrogen electrode; ORR, oxygen reduction reaction; HER, hydrogen evolution reaction

## ■ REFERENCES

(1) Schlapbach, L.; Züttel, A. Hydrogen-Storage Materials for Mobile Applications. *Nature* **2001**, *414* (6861), 353−358.

(2) Hydrogen on the Rise. *Nat. Energy* **2016**, *1*, 16127. .

(3) Chen, P.; Zhu, M. Recent Progress in Hydrogen Storage. *Mater. Today* **2008**, *11* (12), 36−43.

(4) Züttel, A. Materials for Hydrogen Storage. *Mater. Today* **2003**, *6* (9), 24−33.

(5) Jessop, P. Reactions with a Reverse Gear. *Nat. Chem.* **2009**, *1* (5), 350−351.

(6) Target Explanation Document:Onboard Hydrogen Storage for Light-Duty Fuel Cell Vehicles. *U.S. DRIVE*, 2017.https://www.energy.gov/sites/default/files/2017/05/f34/fcto_targets_onboard_hydro_storage_explanation.pdf.

(7) Kato, S.; Saga, Y.; Kojima, M.; Fuse, H.; Matsunaga, S.; Fukatsu, A.; Kondo, M.; Masaoka, S.; Kanai, M. Hybrid Catalysis Enabling Room-Temperature Hydrogen Gas Release from N -Heterocycles and Tetrahydronaphthalenes. *J. Am. Chem. Soc.* **2017**, *139* (6), 2204−2207.

(8) Orimo, S.; Nakamori, Y.; Eliseo, J. R.; Züttel, A.; Jensen, C. M. Complex Hydrides for Hydrogen Storage. *Chem. Rev.* **2007**, *107* (10), 4111−4132.

(9) Rusman, N. A. A.; Dahari, M. A. Review on the Current Progress of Metal Hydrides Material for Solid-State Hydrogen Storage Applications. *Int. J. Hydrogen Energy* **2016**, *41* (28), 12108−12126.

(10) Ley, M. B.; Jepsen, L. H.; Lee, Y.-S.; Cho, Y. W.; Bellosta von Colbe, J. M.; Dornheim, M.; Rokni, M.; Jensen, J. O.; Sloth, M.; Filinchuk, Y.; Jørgensen, J. E.; Besenbacher, F.; Jensen, T. R. Complex Hydrides for Hydrogen Storage − New Perspectives. *Mater. Today* **2014**, *17* (3), 122−128.

(11) Zhu, Q.-L.; Xu, Q. Liquid Organic and Inorganic Chemical Hydrides for High-Capacity Hydrogen Storage. *Energy Environ. Sci.* **2015**, *8* (2), 478−512.

(12) Preuster, P.; Papp, C.; Wasserscheid, P. Liquid Organic Hydrogen Carriers (LOHCs): Toward a Hydrogen-Free Hydrogen Economy. *Acc. Chem. Res.* **2017**, *50* (1), 74−85.

(13) Luo, W.; Campbell, P. G.; Zakharov, L. N.; Liu, S.-Y. A Single-Component Liquid-Phase Hydrogen Storage Material. *J. Am. Chem. Soc.* **2011**, *133* (48), 19326−19329.

(14) Chen, G.; Zakharov, L. N.; Bowden, M. E.; Karkamkar, A. J.; Whittemore, S. M.; Garner, E. B.; Mikulas, T. C.; Dixon, D. A.; Autrey, T.; Liu, S.-Y. Bis-BN Cyclohexane: A Remarkably Kinetically Stable Chemical Hydrogen Storage Material. *J. Am. Chem. Soc.* **2015**, *137* (1), 134−137.

(15) Hull, J. F.; Himeda, Y.; Wang, W.-H.; Hashiguchi, B.; Periana, R.; Szalda, D. J.; Muckerman, J. T.; Fujita, E. Reversible Hydrogen Storage Using CO2 and a Proton-Switchable Iridium Catalyst in Aqueous Media under Mild Temperatures and Pressures. *Nat. Chem.* **2012**, *4* (5), 383−388.

(16) Blankenship II, T. S.; Balahmar, N.; Mokaya, R. Oxygen-Rich Microporous Carbons with Exceptional Hydrogen Storage Capacity. *Nat. Commun.* **2017**, *8* (1), 1545.

(17) Wang, H.; Gao, Q.; Hu, J. High Hydrogen Storage Capacity of Porous Carbons Prepared by Using Activated Carbon. *J. Am. Chem. Soc.* **2009**, *131* (20), 7016−7022.

(18) Xia, G.; Chen, X.; Zhao, Y.; Li, X.; Guo, Z.; Jensen, C. M.; Gu, Q.; Yu, X. High-Performance Hydrogen Storage Nanoparticles Inside Hierarchical Porous Carbon Nanofibers with Stable Cycling. *ACS Appl. Mater. Interfaces* **2017**, *9* (18), 15502−15509.

(19) Yang, S. J.; Kim, T.; Im, J. H.; Kim, Y. S.; Lee, K.; Jung, H.; Park, C. R. MOF-Derived Hierarchically Porous Carbon with Exceptional Porosity and Hydrogen Storage Capacity. *Chem. Mater.* **2012**, *24* (3), 464−470.

(20) Schoedel, A.; Ji, Z.; Yaghi, O. M. The Role of Metal−Organic Frameworks in a Carbon-Neutral Energy Cycle. *Nat. Energy* **2016**, *1* (4), 16034.

(21) Rosi, N. L.; Eckert, J.; Eddaoudi, M.; Vodak, D. T.; Kim, J.; O'Keeffe, M.; Yaghi, O. M. Hydrogen Storage in Microporous Metal-Organic Frameworks. *Science* **2003**, *300* (5622), 1127−1129.

(22) Suh, M. P.; Park, H. J.; Prasad, T. K.; Lim, D.-W. Hydrogen Storage in Metal−Organic Frameworks. *Chem. Rev.* **2012**, *112* (2), 782−835.

(23) Yang, S.; Lin, X.; Blake, A. J.; Walker, G. S.; Hubberstey, P.; Champness, N. R.; Schröder, M. Cation-Induced Kinetic Trapping and Enhanced Hydrogen Adsorption in a Modulated Anionic Metal−Organic Framework. *Nat. Chem.* **2009**, *1* (6), 487−493.

(24) Han, S. S.; Furukawa, H.; Yaghi, O. M.; Goddard, W. A. Covalent Organic Frameworks as Exceptional Hydrogen Storage Materials. *J. Am. Chem. Soc.* **2008**, *130* (35), 11580−11581.

(25) Cao, D.; Lan, J.; Wang, W.; Smit, B. Lithium-Doped 3D Covalent Organic Frameworks: High-Capacity Hydrogen Storage Materials. *Angew. Chem.* **2009**, *121* (26), 4824−4827.

(26) Han, S. S.; Mendoza-Cortés, J. L.; Goddard III, W. A. Recent Advances on Simulation and Theory of Hydrogen Storage in Metal−Organic Frameworks and Covalent Organic Frameworks. *Chem. Soc. Rev.* **2009**, *38* (5), 1460−1476.

(27) Steinfeld, A. Solar Hydrogen Production via a Two-Step Water-Splitting Thermochemical Cycle Based on Zn/ZnO Redox Reactions. *Int. J. Hydrogen Energy* **2002**, *27* (6), 611−619.

(28) Hua, T. Q.; Roh, H.-S.; Ahluwalia, R. K. Performance Assessment of 700-bar Compressed Hydrogen Storage for Light Duty Fuel Cell Vehicles. *Int. J. Hydrogen Energy* **2017**, *42* (40), 25121−25129.

(29) Liu, Z.; Li, C. Influence of Slosh Baffles on Thermodynamic Performance in Liquid Hydrogen Tank. *J. Hazard. Mater.* **2018**, *346* (40), 253−262.

(30) Stern, A. G. Design of an Efficient, High Purity Hydrogen Generation Apparatus and Method for a Sustainable, Closed Clean Energy Cycle. *Int. J. Hydrogen Energy* **2015**, *40* (32), 9885−9906.

(31) Martinez Julca, M. A.; Rivera, I.; Perales-Perez, O.; Bailon, S.; Perez, M. Li-Doped ZnO Nanoparticles as Novel Direct Generator of Singlet Oxygen for Potential Photodynamic Therapy Applications. *Mater. Res. Soc. Symp. Proc.* **2015**, *1784* (April 2016), 1−6.

(32) Abirami, M.; Hwang, S. M.; Yang, J.; Senthilkumar, S. T.; Kim, J.; Go, W.-S.; Senthilkumar, B.; Song, H.-K.; Kim, Y. A Metal−Organic Framework Derived Porous Cobalt Manganese Oxide Bifunctional Electrocatalyst for Hybrid Na−Air/Seawater Batteries. *ACS Appl. Mater. Interfaces* **2016**, *8* (48), 32778−32787.

(33) Hwang, S. M.; Park, J.; Kim, Y.; Go, W.; Han, J.; Kim, Y.; Kim, Y. Rechargeable Seawater Batteries—From Concept to Applications. *Adv. Mater.* **2019**, *31* (20), 1804936.

(34) Kim, J.-K.; Mueller, F.; Kim, H.; Bresser, D.; Park, J.-S.; Lim, D.-H.; Kim, G.-T.; Passerini, S.; Kim, Y. Rechargeable-Hybrid-Seawater Fuel Cell. *NPG Asia Mater.* **2014**, *6* (11), No. e144.

(35) Kang, S. J.; Mori, T.; Narizuka, S.; Wilcke, W.; Kim, H.-C. Deactivation of Carbon Electrode for Elimination of Carbon Dioxide Evolution from Rechargeable Lithium−Oxygen Cells. *Nat. Commun.* **2014**, *5* (1), 3937.

(36) Zhu, Y.; Suo, L.; Gao, T.; Fan, X.; Han, F.; Wang, C. Ether-Based Electrolyte Enabled Na/FeS2 Rechargeable Batteries. *Electrochem. Commun.* **2015**, *54*, 18−22.

(37) Hu, Z.; Zhu, Z.; Cheng, F.; Zhang, K.; Wang, J.; Chen, C.; Chen, J. Pyrite FeS 2 for High-Rate and Long-Life Rechargeable Sodium Batteries. *Energy Environ. Sci.* **2015**, *8* (4), 1309−1316.

(38) Davis, R. E.; Sherman, J. T. Evaluating a Lithium-Seawater Battery on Gliders. *J. Atmos. Ocean. Technol.* **2017**, *34* (5), 1175−1182.

(39) Kim, Y.; Harzandi, A. M.; Lee, J.; Choi, Y.; Kim, Y. Design of Large-Scale Rectangular Cells for Rechargeable Seawater Batteries. *Adv. Sustain. Syst.* **2021**, *5*, 2000106.

(40) Nørskov, J. K.; Rossmeisl, J.; Logadottir, A.; Lindqvist, L.; Kitchin, J. R.; Bligaard, T.; Jónsson, H. Origin of the Overpotential for Oxygen Reduction at a Fuel-Cell Cathode. *J. Phys. Chem. B* **2004**, *108* (46), 17886−17892.

(41) Jiang, Y.; Yang, L.; Sun, T.; Zhao, J.; Lyu, Z.; Zhuo, O.; Wang, X.; Wu, Q.; Ma, J.; Hu, Z. Significant Contribution of Intrinsic Carbon Defects to Oxygen Reduction Activity. *ACS Catal.* **2015**, *5* (11), 6707−6712.

(42) Jia, Y.; Zhang, L.; Zhuang, L.; Liu, H.; Yan, X.; Wang, X.; Liu, J.; Wang, J.; Zheng, Y.; Xiao, Z.; Taran, E.; Chen, J.; Yang, D.; Zhu, Z.; Wang, S.; Dai, L.; Yao, X. Identification of Active Sites for Acidic Oxygen Reduction on Carbon Catalysts with and without Nitrogen Doping. *Nat. Catal.* **2019**, *2* (8), 688−695.

(43) Kim, J. K.; Lee, E.; Kim, H.; Johnson, C.; Cho, J.; Kim, Y. Rechargeable Seawater Battery and Its Electrochemical Mechanism. *ChemElectroChem* **2015**, *2* (3), 328−332.

(44) Ha, M.; Kim, D. Y.; Umer, M.; Gladkikh, V.; Myung, C. W.; Kim, K. S. Tuning Metal Single Atoms Embedded in NxCy Moieties toward High-Performance Electrocatalysis. *Energy Environ. Sci.* **2021**, *14* (6), 3455−3468.

(45) Tiwari, J. N.; Sultan, S.; Myung, C. W.; Yoon, T.; Li, N.; Ha, M.; Harzandi, A. M.; Park, H. J.; Kim, D. Y.; Chandrasekaran, S. S.; Lee, W. G.; Vij, V.; Kang, H.; Shin, T. J.; Shin, H. S.; Lee, G.; Lee, Z.; Kim, K. S. Multicomponent Electrocatalyst with Ultralow Pt Loading and High Hydrogen Evolution Activity. *Nat. Energy* **2018**, *3* (9), 773−782.

(46) Cao, H.; Li, Z.; Xie, Y.; Xiao, F.; Wang, H.; Wang, X.; Pan, K.; Cabot, A. Hierarchical CoP Nanostructures on Nickel Foam as Efficient Bifunctional Catalysts for Water Splitting. *ChemSusChem* **2021**, *14* (4), 1094−1102.

(47) Li, Y. K.; Zhang, G.; Lu, W. T.; Cao, F. F. Amorphous Ni−Fe−Mo Suboxides Coupled with Ni Network as Porous Nanoplate Array on Nickel Foam: A Highly Efficient and Durable Bifunctional Electrode for Overall Water Splitting. *Adv. Sci.* **2020**, *7* (7), 1902034.

(48) Millero, F. J.; Feistel, R.; Wright, D. G.; McDougall, T. J. The Composition of Standard Seawater and the Definition of the Reference-Composition Salinity Scale. *Deep Sea Res., Part I* **2008**, *55* (1), 50−72.

(49) Wieser, M. E. Atomic Weights of the Elements 2005 (IUPAC Technical Report). *Pure Appl. Chem.* **2006**, *78* (11), 2051−2066.

(50) Melaina, M.; Penev, M.; Heimiller, D. Resource Assessment for Hydrogen Production Hydrogen Production Potential from Fossil and Renewable Energy Resources, 2013. https://www.nrel.gov/docs/fy13osti/55626.pdf.